Journal of King Saud University – Science 32 (2020) 1359–1365

Contents lists available at ScienceDirect

Journal of King Saud University – Science

journal homepage: www.sciencedirect.com

Original article

Facile fabrication of chitosan-*cl*-poly(AA)/$ZrPO_4$ nanocomposite for remediation of rhodamine B and antimicrobial activity

Gaurav Sharma [a,b,*], Mu. Naushad [c], Amit Kumar [a], Ashok Kumar [d], Tansir Ahamad [c], Florian J. Stadler [a]

[a] College of Materials Science and Engineering, Shenzhen Key Laboratory of Polymer Science and Technology, Guangdong Research Center for Interfacial Engineering of Functional Materials, Nanshan District Key Lab for Biopolymers and Safety Evaluation, Shenzhen University, Shenzhen 518055, PR China
[b] School of Chemistry, Shoolini University, Solan 173212, Himachal Pradesh, India
[c] Department of Chemistry, College of Science, Bld.#5, King Saud University, Riyadh, Saudi Arabia
[d] Department of Biotechnology and Bioinformatics, Jaypee University of Information Technology, Waknaghat, Solan, Himachal Pradesh 173234, India

ARTICLE INFO

Article history:
Received 30 September 2019
Revised 14 November 2019
Accepted 19 November 2019
Available online 27 November 2019

Keywords:
Nanocomposite
Zirconium Phosphate
Chitosan
Photocatalysis
Antimicrobial

ABSTRACT

The chitosan based nanohydrogel reinforced nanocomposite was fabricated by facile sol–gel polymerization technique. A chitosan-cl-poly(AA)/$ZrPO_4$ nanocomposite was discovered as a capable photocatalyst for the elimination of rhodamine dye. The designed chitosan-cl-poly(AA)/$ZrPO_4$ nanocomposite was examined by various characterization approaches such as Scanning electron microscopy (SEM), X-Ray diffraction (XRD), Fourier-transform infrared spectroscopy (FTIR) and Transmission electron microscopy (TEM). The photocatalytic experiment outcomes revealed that the nanocomposite had good remediation potential as 82% of rhodamine B dye was remediated within 3 h of process. The antimicrobial behavior of nanocomposite was studied against *Pseudomonas aeruginosa, Escherichia coli* and *Staphylococcus aureus* bacteria. Cell toxicity of the synthesized chitosan-cl-poly(AA)/ZrPO4 nanocomposite was performed against *Vibrio fischeri* as model organism. The chitosan-cl-poly(AA)/$ZrPO_4$ nanocomposite demonstrated the potential antibacterial behavior.

1. Introduction

Owing to extraordinary progress in urbanization and industrialization, the environmental contamination has been a great fear in present context of times. Pollution is the entrance of pollutes into the natural atmosphere that causes hostile change. Huge amount of carbon-based and inorganic contaminants has been introduced within water bodies from domestic and industrial sources (Ghorai et al., 2014; Hosseini Asl et al., 2019). Constituents of contaminates, can be either foreign substances or naturally happening pollutants. The carbon-based pollutants such as insecticides, phenols and colorants etc. causes various stern threats to the atmosphere and human well-being (Motshekga et al., 2015; Sharma et al., 2017; Zhang and Wang, 2010). The above contaminants have been released from the different industries as fabric, paper & pulp, medical, paint, bleaching and tannery etc. To unravel this problem, manufacturing industries waters must be treated to confiscate the noxious pollutants previously they are released into the water sources. Several chemical and physical procedures have been established and are active for environmental remediation such as coagulation, adsorption, reverse osmosis, extraction, chemical precipitation, ion exchange, membrane filtration, and photocatalysis etc. (Lei et al., 2019; Naushad, 2014; Sharma et al., 2015). The tenacious carbon-based pollutants have stern health threats and essential be detached before receiving into water, air and soil. Development of these carbon-based pollutants released from manufacturing effluents over time period in the bodies of living beings can root serious impairment as these cannot be remediated biologically. The existence of contaminants above acceptable quantities in environment can be reasons for health issues as abdominal pain, liver impairment, breathing problems, gastrointestinal bleeding, kidney disfunction and even cancer in organisms, etc. (Al-Ghouti et al., 2003). Photocatalysis is one of the existing procedures active for the exclusion of pollutants from

* Corresponding author at: College of Materials Science and Engineering, Shenzhen Key Laboratory of Polymer Science and Technology, Guangdong Research Center for Interfacial Engineering of Functional Materials, Nanshan District Key Lab for Biopolymers and Safety Evaluation, Shenzhen University, Shenzhen 518055, PR China.
E-mail address: gaurav8777@gmail.com (G. Sharma).

Peer review under responsibility of King Saud University.

Production and hosting by Elsevier

https://doi.org/10.1016/j.jksus.2019.11.028
1018-3647/

environment, and still has its enormous significance in the coming eras (Cheng et al., 2016). With the stable evolutions of varied photocatalyst materials, the arena of photocatalysis has become wider and explicit in nature for precise pollutants encompassing antibiotics, heavy metals, dyes, phenols and insecticides etc. The number of photocatalyst of higher photocatalytic competence and selectivity have been produced, e.g. metal oxides, bimetallic and trimetallic nanoparticles, ferrites, metal sulphides, nanocomposites and metal organic frameworks (MOFs) (Fresno et al., 2014; Sharma et al., 2018a; Sharma et al., 2019). Out of these the nanocomposites have shown extraordinary role in photocatalysis, and are widely explored for exclusion of carbon-based pollutants from wastewater due to their numerous advantages. Such as their organic counterpart provides the large surface for attachment of inorganic part hence increase its mechanical strength and also increase its adsorption capacity (Zhang et al., 2014). The various organic materials used in preparation of nanocomposites includes, graphene, carbon nitrides and biopolymers etc. The combination of nanoparticles with polymers and hydrogels is a new and quickly emerging class of materials, gaining extensive application in several areas, chiefly in pharmacy, agriculture and environmental remediation (Sharma et al., 2018c; Sui et al., 2019; Vanaamudan et al., 2018). Biopolymers are specially focused materials for fabrication of hydrogels, nanofibers, biopolymeric microspheres and nanospheres as these are easily available and biocompatible in nature. Crosslinked hydrophilic biopolymeric hydrogels matrix are among the most promising supports for synthesis of their nanocomposites with inorganic materials as their three-dimensional network provides suitable sites for attachment, and even their properties can be tailored by simple modifying the functionalities in their structure (Prusty and Swain, 2018).

Thus, nanohydrogels are used to improve the properties of pre synthesized inorganic particles (Naushad et al., 2019). Nature has unceasingly joined organic and inorganic constituents, on the nanoscale, to create smart materials with amazing functions and properties (mechanics, density, colour, hydrophobicity, permeability etc.). Nanocomposites hydrogels are composed of nanosized inorganic particles mixed with some organic matrix these have greater surface area and the particles at interface adopts key roles, as these explains their final properties. Currently, nanocomposites have virtuous future perceptions, where using these, exigent and novel applications are executed to accomplish enormous harmony among human actions and environment (Packirisamy et al., 2019; Rabel et al., 2019; Sharma et al., 2014; Singh et al., 2019).

The present work provides an insight into fabrication of zirconium phosphate embedded chitosan-based nanocomposite fabricated by simple sol–gel method. Thus nanocomposite was explored for its photocatalytic and antimicrobial action.

2. Materials and techniques

2.1. Chemicals and instruments

Zirconium oxychloride, orthophosphoric acid, acetic acid, ammonium per sulfate purchased from CDH Pvt. Ltd. India. Aliginic acid was attained from Loba Chemie Pvt. Ltd. India. *N,N'*-methylene bisacryl amide was purchased from S-D fine Chem. Limited, India.

Shaker, Centrifuge machine (Instruments, Chemical Private Limited), Fourier transform infrared (FTIR) spectrophotometer (Nicolet 5700 FTIR Spectrophotometer), X-Ray Diffractrometer (Philips 1830 diffractometer), UV–visible spectrometer (INCO Instrument and Chemical Private Limited), Transmission electron microscopy (Techni G2 20 S-Twin), Scanning electron microscopy (JSM 6100) were used here.

2.2. Synthesis of chitosan-cl-poly(AA)/$ZrPO_4$ nanocomposite

The nanocomposite was fabricated by means of sol–gel/polymerization method. Inorganic counterpart was synthesized by mixing 0.05 M orthophosphoric acid dropwise into 0.1 M zirconium oxchloride solution with continuous stirring. The obtained sol of zirconium phosphate was reserved in mother liquor for about 24 h for complete digestion. Chitosan-cl-poly(AAc) was synthesized as discussed in our previous works (Sharma et al., 2017). The sol of zirconium phosphate was added into the prepared gel of chitosan-cl-poly(AAc). To the above blend, ammonium persulfate (initiator) and *N,N'*–methylene bisacyrlamide (crosslinker) were added. The subsequent blend was stirred for 6 h at 70 °C by means of magnetic stirrer. The obtained chitosan-*cl*-poly(AAc)/$ZrPO_4$ nanocomposite was collected with ethanol. Subsequently, the resulting material was washed numerous times using water–ethanol. Lastly, the nanocomposite was dried under inert conditions in nitrogen atmosphere at 50 °C.

2.3. Characterization

The Fourier Transform Infrared (FTIR) spectrum of chitosan-*cl*-poly(AAc)/$ZrPO_4$ nanocomposite was studied using FTIR (Nicolet 5700 FTIR Spectrophotometer). For FTIR, chitosan-*cl*-poly(AAc)/$ZrPO_4$ nanocomposite was powdered and mixed with KBr to make pellets and spectrum was noted. X-ray diffraction pattern was logged using a Philips 1830 diffractometer. The surface topographies of chitosan-*cl*-poly(AAc)/$ZrPO_4$ nanocomposite was considered using JSM 6100 scanning electron microscope. Sample was mounted rigidly on a specimen holder. The dimensional analysis was done using transmission electron microscopy (Techni G2 20 S-Twin). The nanocomposite was ultrasonicated for 2 h in ethanol and was loaded on carbon grid and examined under the TEM instrument below different resolutions. For determination of the optical band gap of chitosan-*cl*-poly(AAc)/$ZrPO_4$ nanocomposite a suspension of it was made in ethanol. The suspension was then ultrasonicated for 90 min. The UV–vis spectrum of suspension was attained by employing double-beam spectrophotometer and Tauc relation is used for calculating the direct band gap.

2.4. Rhodamine B photocatalytic degradation

The photocatalytic nature of chitosan-*cl*-poly(AAc)/$ZrPO_4$ nanocomposite was tested for the degradation of rhodamine B dye. The photocatalytic tests were achieved using photoreactor surrounded with thermostatic water current to maintain a 25 °C ± 1 continual temperature. Chitosan-*cl*-poly(AAc)/$ZrPO_4$ nanocomposite(100 mg) was inserted into 2×10^{-6} M solution of rhodamine B dye to make a slurry. Firstly, the slurry was set aside in dark to reach the adsorption–desorption steadiness and later uncovered to sunlight for further photocatalysis. Approximately 4 mL of the rhodamine B solution was taken out at numerous breaks of period and centrifuged to impound particles of chitosan-*cl*-poly(AAc)/$ZrPO_4$ nanocomposite. The absorbance was noted in the range of 300–750 nm and kinetics for the photocatalytic degradation of rhodamine B was inspected at 554 nm. Following above procedure, the reusability study was performed for five consecutive cycles. The percent degradation of rhodamine B was found as (Gupta et al., 2015; Rupa et al., 2007):

$$\% \text{ degradation} = \frac{C_0 - C_t}{C_0} x100 \quad (1)$$

where, C_0 and C_t are the concentrations of rhodamine B at equilibrium and at time t. The chemical oxygen demand (COD) was assessed using Chemetrics low range COD vials.

2.5. Antimicrobial activity and cell toxicity of chitosan-cl-poly(AAc)/$ZrPO_4$ nanocomposite

The antibacterial activity of the synthesized chitosan-*cl*-poly (AAc)/$ZrPO_4$ nanocomposite was analyzed against *Pseudomonas aeruginosa, Escherichia coli* and *Staphylococcus aureus* as described previously(Travan et al., 2009). The nanocomposite preparations were sterilized at 121 °C for 20 min. The selected cultures were grown overnight at 37 °C under continuous shaking at 150 rpm. The colony forming unites were counted on the tested plates with added chitosan-*cl*-poly(AAc)/$ZrPO_4$ nanocomposite and without chitosan-*cl*-poly(AAc)/$ZrPO_4$ nanocomposite as control.

The cell toxicity of the synthesized chitosan-*cl*-poly(AAc)/$ZrPO_4$ nanocomposite was performed by using Microtox machine and the study was performed against *Vibrio fischeri* as model organism. The toxicity analysis was done by toxicity test protocol. chitosan-*cl*-poly(AAc)/$ZrPO_4$ nano-composite (5.0 mg/mL) was suspended in double distilled water, to form a homogenous mixture and osmotic adjusting solution were added. The endpoint obtained by the Microtox assay, which notices the decrease in the light intensity emanated by the luminescent bacterium *V. fischeri* afterward the exposure for 15 and 30 min (Hira et al., 2018).

3. Result and discussion

3.1. Synthesis and characterization of chitosan-cl-poly(AAc)/$ZrPO_4$ nanocomposite

The chitosan-*cl*-poly(AAc)/$ZrPO_4$ nanocomposite has been synthesized using sol–gel polymerization process in existence of crosslinker *N,N'*-methylene bis-acyrlamide. The reaction yield for synthesis of chitosan-*cl*-poly(AAc)/$ZrPO_4$ nanocomposite was found to and 88%. The FTIR spectrum Fig. 1(a) shows the characteristics peaks in chitosan-*cl*-poly(AAc)/$ZrPO_4$ nanocomposite. The peaks signals at 1114 cm^{-1}, 1589 $cm^{-1}$and 3390 $cm^{-1}$are assigned to the C–O stretching, C = O stretching and O–H stretching vibrations for the chitosan molecules (Sharma et al., 2018b; Sharma et al., 2017). The representative peak at 1051 cm^{-1} is for ionic phosphate stretching Fig. 1(a). The peak that detected at about 2347 cm^{-1} is recognized to the manifestation of C–H bond. A broad band from 650 to 500 cm^{-1} at is due to the presence of metal oxide connection (Bhatt et al., 2019).

X-ray diffraction pattern of chitosan-*cl*-poly(AAc)/$ZrPO_4$ nanocomposite was revealed in Fig. 1(b). The peaks at 2θ = 11.5°, 19.8° and 24.7° and 28.7° represents the presence of zirconium phosphate with diffraction planes (0 0 2) (1 1 0) and (1 1 2) (Fu et al., 2018), whereas the peaks at 2θ = 31.8°, 33.5°, 38.2, 48.5, 54.1° and 59.2° reveal the presence of Zr-O linkage of zirconium phosphate with chitosan-cl-poly(AAc) counterpart conforming to diffraction planes of (1 1 1), (2 0 0), (2 2 0) and (3 1 1) correspondingly (JCPDS file no. 27–0997) (Kumar et al., 2016). The presence of low intensity small peaks overlapping around 2θ = 10° and 20° confirmed presence of chitosan-*cl*-poly(AAc)counterpart (Kumar and Koh, 2012). Therefore, the XRD results confirm the formation of chitosan-*cl*-poly(AAc)/$ZrPO_4$ nanocomposite. Surface micrographs of chitosan-*cl*-poly(AAc)/$ZrPO_4$ nanocomposite was considered by means of scanning electron microscope. Fig. 2. (a, b, c and d) displays the SEM images of chitosan-*cl*-poly(AAc)/$ZrPO_4$ nanocomposite at different magnification. Pictures reveals that dur to presence of $ZrPO_4$ the surface morphology of nanocomposite appears to be irregular with rough texture. Thus SEM reveals the presence of both components in chitosan-*cl*-poly(AAc)/$ZrPO_4$ nanocomposite i.e., $ZrPO_4$ and chitosan-*cl*-poly(AAc). TEM images of chitosan-*cl*-poly(AAc)/$ZrPO_4$ nanocomposite are shown in Fig. 3.(a and b) at diverse magnification. TEM pictures indicated appearance of $ZrPO_4$ embedded in matrix of chitosan-*cl*-poly(AAc) with average size of particles between 30 and 70 nm. Fig. 4 depicts that the optical band gap of chitosan-*cl*-poly(AAc)/$ZrPO_4$ nanocomposite is 3.1 eV which lies in ultraviolet regions for semiconductors hence nanocomposite can be explored for its photocatalytic nature.

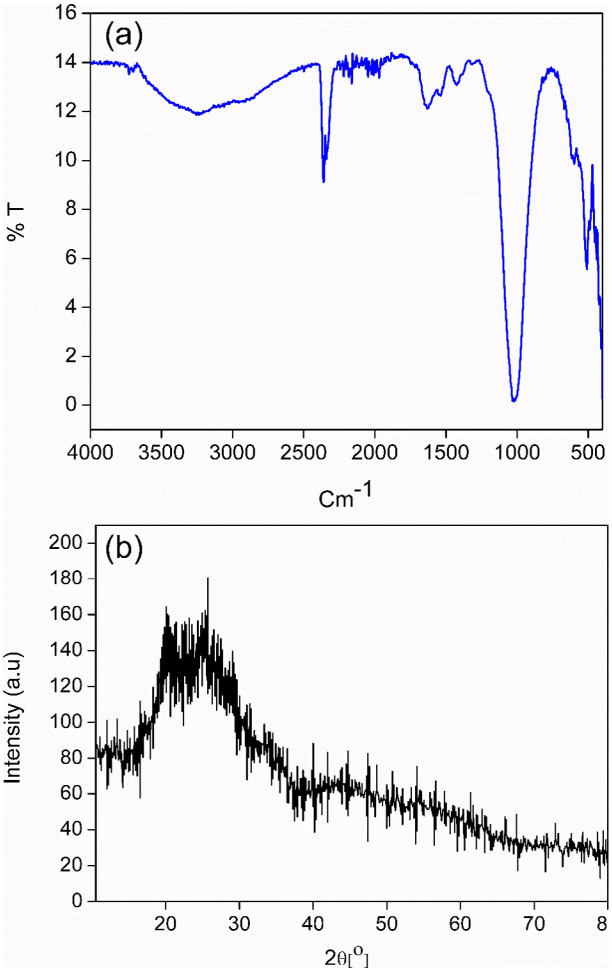

Fig. 1. (a) FTIR spectrum (b) XRD pattern of chitosan-*cl*-poly(AA)/$ZrPO_4$ nanocomposite.

3.2. Photocatalytic degradation of rhodamine B

Photocatalytic degradation of the rhodamine B dye using chitosan-*cl*-poly(AAc) nanocomposite is shown in Fig. 5(a, b and c). Fig. 5(a) decapitates the change in absorbance with exposer period. The progression of photocatalytic activity befalls in two steps; adsorption–desorption equilibrium and photocatalysis. It was detected that maximum 20% of rhodamine B dye get adsorbed after one hour of contact period to achieve equilibrium and 62% of dye undergoes photocatalysis in 2 h of photoperiod and it was observed that about 82% of the rhodamine B dye was removed within 3 h of complete process Fig. 5 (b). The rate of photocatalytic degradation of rhodamine B dye was reported to follow pseudo first order kinetic model:

$$r = \frac{dc}{dt} = K_{app}t \tag{2}$$

$$ln\frac{C_0}{C_t} = K_{app}t \tag{3}$$

where k_{app} is the apparent rate constant, C_0 is the concentration of rhodamine B before illumination and C_t is the concentration of rho-

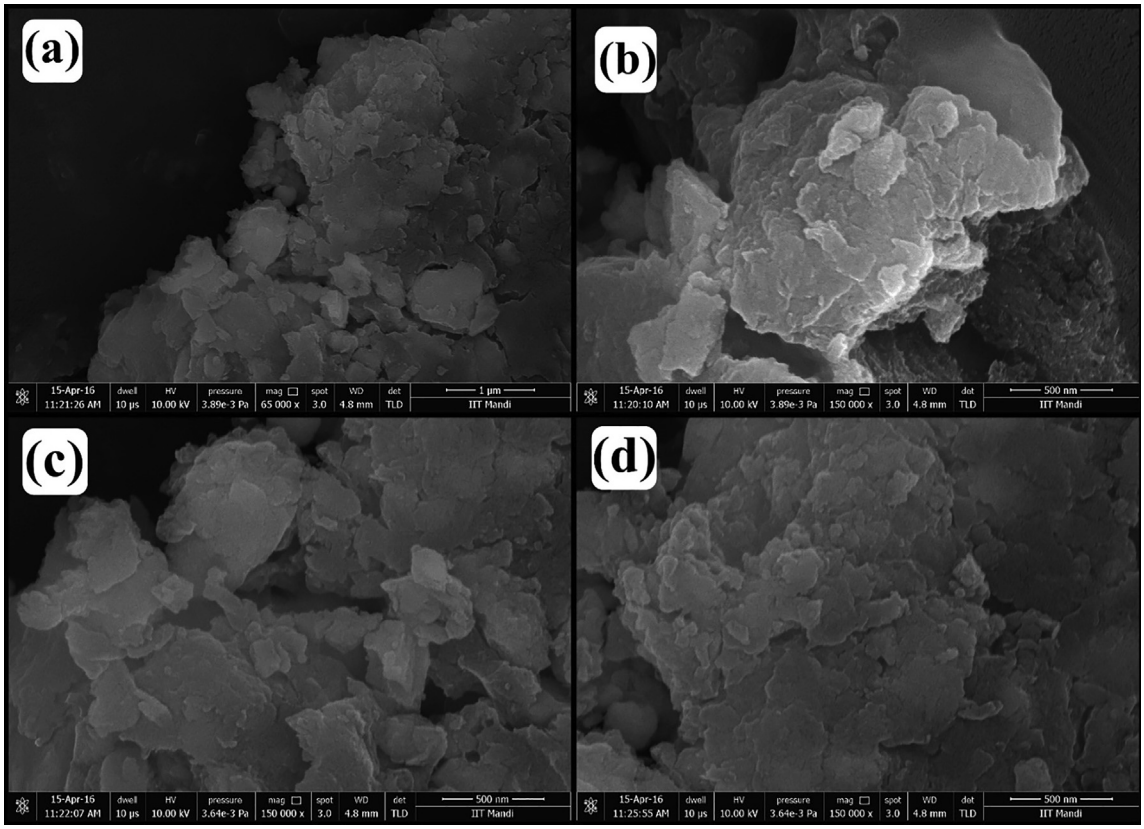

Fig. 2. SEM images of chitosan-*cl*-poly(AA)/$ZrPO_4$ nanocomposite.

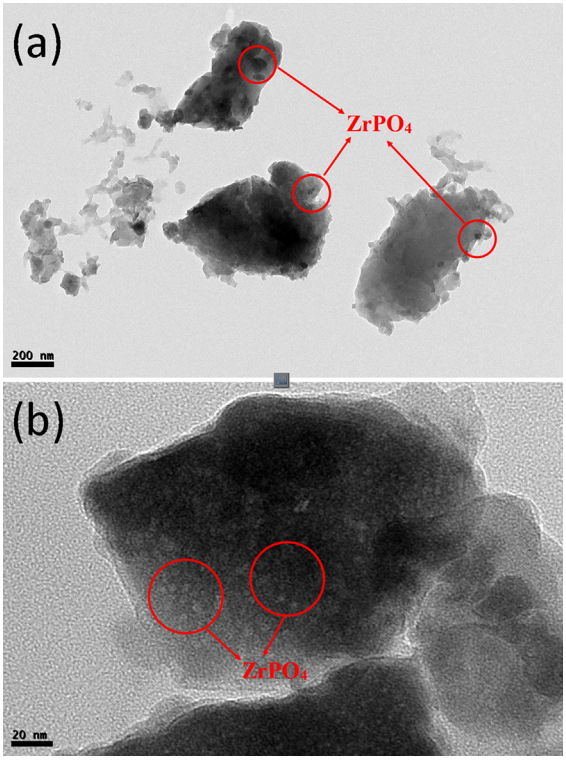

Fig. 3. TEM images of chitosan-*cl*-poly(AA)/$ZrPO_4$ nanocomposite.

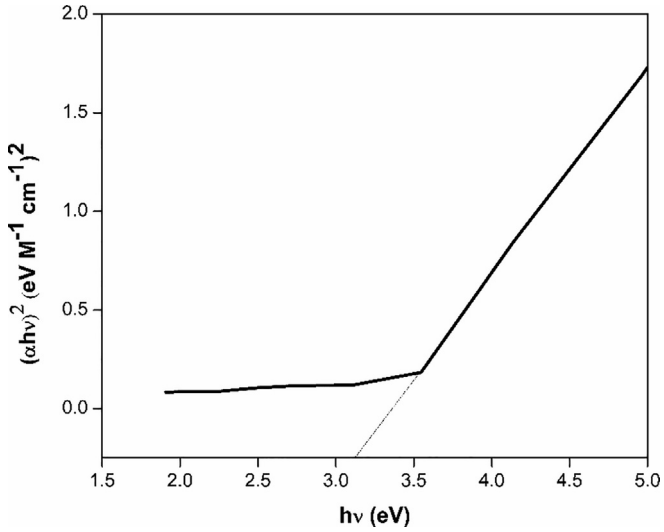

Fig. 4. Band Gap of chitosan-*cl*-poly(AA)/$ZrPO_4$ nanocomposite.

damine B at time t. The value of rate constant was found to be 0.002 min^{-1} and R^2 is 0.99713. The chitosan-cl-poly(AAc) part is responsible for the adsorption of rhodamine B dye whereas $ZrPO_4$ acted as photocatalysts. The electron-hole pair generates when sunlight interact with metallic particles of nanocomposite. These electron-hole pair further produce superoxide anion radicals or hydroxyl radicals by series of reactions (Boughelout et al., 2018; Ghafuri et al., 2019; Mehrabian and Esteki, 2017). These superoxide anion radicals or hydroxyl radicals are accountable for degradation of rhodamine B.

The removal efficiency of chitosan-cl-poly(AAc)/$ZrPO_4$ nanocomposite for dye was also examined by chemical oxygen

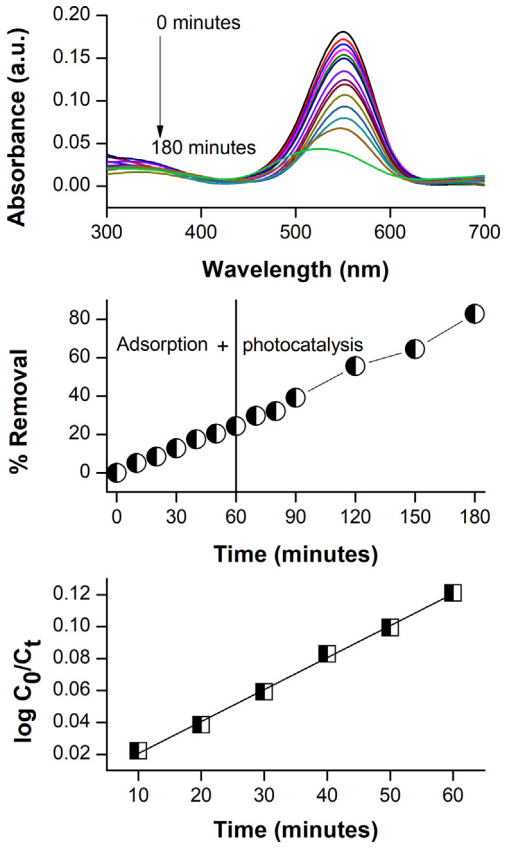

Fig. 5. (a) Absorbance spectra for degradation of rhodamine B dye by chitosan-cl-poly(AAc)/$ZrPO_4$ nanocpmposite (b) percent degradation of rhodamine B (c) kinetics for degradation process.

demand (COD) investigation. The COD is an active procedure to quantify the concentration of organic matter existing in reaction. The COD examination allows to measure total amount of oxygen essential for the complete oxidation of organic content to carbon dioxide and water (Meng et al., 2019; Priya and Jeyanthi, 2019). Fig. 6(a) displays the decrease in COD of dye solution at several reaction intervals. The COD of reaction solution lowered to 39% in 3 h indicating noteworthy mineralization of dye. The reusability of chitosan-cl-poly(AAc)/$ZrPO_4$ nanocomposite was investigated for consecutive 5 cycles and it was detected that after 5th cycle 61% dye was remediated (Fig. 6b). Thus, proving effectiveness of nanocomposite for multiple use.

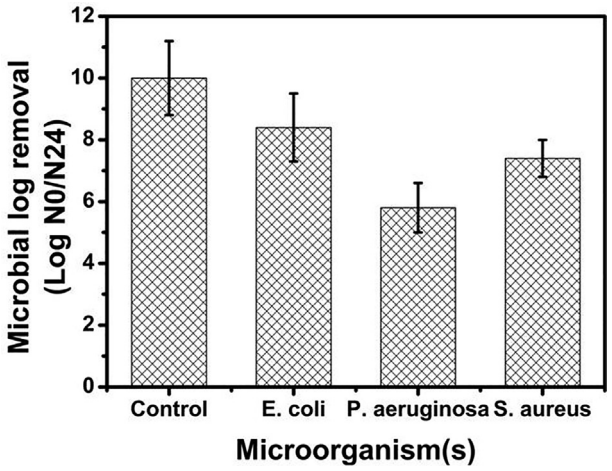

Fig. 7. Antimicrobial activities of chitosan-*cl*-poly(AAc)/$ZrPO_4$ nanocomposite.

3.3. Antimicrobial activity and cell toxicity and chitosan-cl-poly(AAc)/$ZrPO_4$ nanocomposite

The antibacterial activities of the synthesized chitosan-*cl*-poly(AAc)/$ZrPO_4$ nanocomposite was analyzed against *Pseudomonas aeruginosa, Escherichia coli* and *Staphylococcus aureus* as described previously. The results exhibited that the antimicrobial activity of chitosan-*cl*-poly(AAc)/$ZrPO_4$ is higher towards all tested microorganisms (Fig. 7). Whereas *E.coli* strain was found to be much more resistant than that of *S. aureus* and *P. aeruginosa*. In a previous report, the nanocomposite of cellulose and copper were tested for their antimicrobial action against *Klebsiella pneumoniae and Staphylococcus aureus* , which showed morphology and concentration of metal content affect the antibacterial activity (Pinto et al., 2013). In another study, a chitosan nanocomposite with Ag nanoparticles showed high antimicrobial action against *S. aureus*, *P. aeruginosa, Candida albicans and E. coli*. Thus, presence of chitosan and $ZrPO_4$ nanoparticles make our nanocomposite as promising antibacterial agent.

The cell toxicity of the synthesized chitosan-*cl*-poly(AAc)/$ZrPO_4$ was performed by using 81.9% toxicity test. The acute toxicity (EC_{50}) values of chitosan-*cl*-poly(AAc)/$ZrPO_4$ nanocomposite were 257 and 121 μg/mL towards the *V. fischeri* after 15 and 30 min of incubation (Table 1). The significantly higher EC_{50} values for chitosan-cl-poly(AAc)/$ZrPO_4$ detected herein demonstrates the more biocompatible nature of synthesized nanocomposite. Literature studies suggested that reactive oxygen species generated by

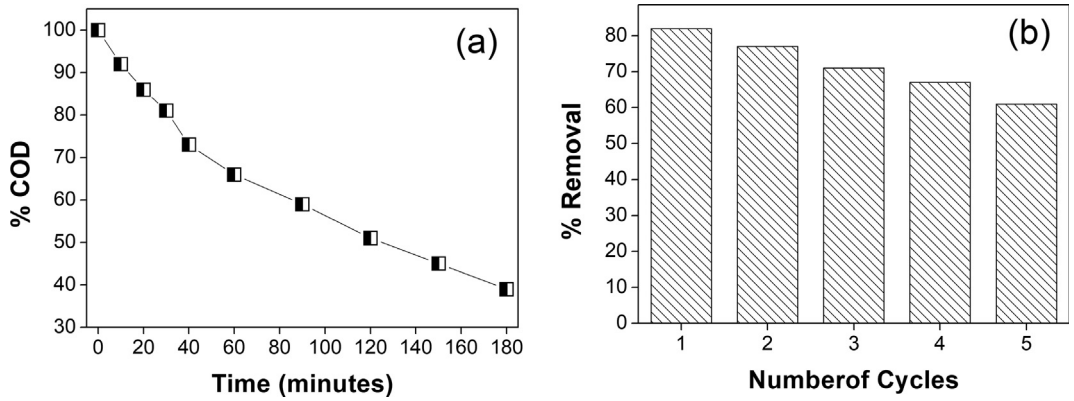

Fig. 6. (a) COD for degradation of rhodamine B dye by chitosan-cl-poly(AAc)/$ZrPO_4$ nanocpmposite (b) reusability.

Table 1
Effect of incubation of chitosan-cl-poly(AAc)/$ZrPO_4$ nanocomposite with *Vibrio fischeri* for 15 and 30 min in Microtox for acute toxicity analysis.

Type of particles	parameter	EC_{50} value (μg/mL)
chitosan-cl-poly(AA)/$ZrPO_4$	$EC_{50\text{-}15min}$	257 ± 0.32
	$EC_{50\text{-}30min}$	121 ± 0.41

nanoparticles are responsible for toxicity. Generally the toxicity of nanoparticles depends on amount of dose, size, and type of cell (Regiel-Futyra et al., 2017). Hence, in our study we found that our chitosan-cl-poly(AAc)/$ZrPO_4$ nanocomposite is nontoxic and biocompatible in nature.

4. Conclusion

Novel hydrogel-based nanocomposite was fabricated by simplistic sol–gel/polymerization method. The chitosan-cl-poly(AAc)/$ZrPO_4$ was successfully used for remediation of rhodamine B dye from aqueous medium. The particle diameter lies between 30 and 70 nm for $ZrPO_4$. Diverse characterization procedures verified the fabrication of the nanocomposites. The percent remediation for rhodamine B was found to be 82%. The chitosan-cl-poly(AAc)/$ZrPO_4$ was tested for its antimicrobial activity against different bacteria's. It was observed that chitosan-cl-poly(AAc)/$ZrPO_4$ nanocomposite showed promising antibacterial nature. On the other hand, cytotoxicity studies reveled that nanocomposite was non-toxic and biocompatible. Thus, chitosan-cl-poly(AAc)/$ZrPO_4$ nanocomposite with desirable properties is useful material for wastewater treatment.

Acknowledgment

One of the authors (Mu. Naushad) is grateful to the Researchers Supporting Project number (RSP-2019/8), King Saud University, Riyadh, Saudi Arabia for the support. The financial support from China Postdoctoral Science Foundation Grant (2018M643168) is greatly acknowledged.

References

Al-Ghouti, M.A., Khraisheh, M.A.M., Allen, S.J., Ahmad, M.N., 2003. The removal of dyes from textile wastewater: a study of the physical characteristics and adsorption mechanisms of diatomaceous earth. J. Environ. Manage. 69 (3), 229–238.

Bhatt, R., V, A., Rathod, S.B., P, P., 2019. Self-assembled chitosan-zirconium phosphate nanostructures for adsorption of chromium and degradation of dyes. Carbohydrate Polymers 208, 441-450

Boughelout, A., Zebbar, N., Macaluso, R., Zohour, Z., Bensouilah, A., Zaffora, A., Aida, M.S., Kechouane, M., Trari, M., 2018. Rhodamine (B) photocatalysis under solar light on high crystalline ZnO films grown by home-made DC sputtering. Optik 174, 77–85.

Cheng, G., Xu, F., Xiong, J., Tian, F., Ding, J., Stadler, F.J., Chen, R., 2016. Enhanced adsorption and photocatalysis capability of generally synthesized TiO_2-carbon materials hybrids. Adv. Powder Technol. 27 (5), 1949–1962.

Fresno, F., Portela, R., Suárez, S., Coronado, J.M., 2014. Photocatalytic materials: recent achievements and near future trends. J. Mater. Chem. A 2 (9), 2863–2884.

Fu, X.-L., Wang, X., Xing, W., Zhang, P., Song, L., Hu, Y., 2018. Two-dimensional cardanol-derived zirconium phosphate hybrid as flame retardant and smoke suppressant for epoxy resin. Polym. Degrad. Stab. 151, 172–180.

Ghafuri, H., Dehghani, M., Rashidizadeh, A., Rabbani, M., 2019. Synthesis and characterization of magnetic nanocomposite Fe_3O_4@TiO_2/Ag, Cu and investigation of photocatalytic activity by degradation of rhodamine B (RhB) under visible light irradiation. Optik 179, 646–653.

Ghorai, S., Sarkar, A., Raoufi, M., Panda, A.B., Schönherr, H., Pal, S., 2014. Enhanced Removal of Methylene Blue and Methyl Violet Dyes from Aqueous Solution Using a Nanocomposite of Hydrolyzed Polyacrylamide Grafted Xanthan Gum and Incorporated Nanosilica. ACS Appl. Mater. Interfaces 6 (7), 4766–4777.

Gupta, V.K., Saleh, T.A., Pathania, D., Rathore, B.S., Sharma, G., 2015. A cellulose acetate based nanocomposite for photocatalytic degradation of methylene blue dye under solar light. Ionics 21 (6), 1787–1793.

Hira, I., Kumar, A., Kumari, R., Saini, A.K., Saini, R.V., 2018. Pectin-guar gum-zinc oxide nanocomposite enhances human lymphocytes cytotoxicity towards lung and breast carcinomas. Mater. Sci. Eng., C 90, 494–503.

Hosseini Asl, S.M., Javadian, H., Khavarpour, M., Belviso, C., Taghavi, M., Maghsudi, M., 2019. Porous adsorbents derived from coal fly ash as cost-effective and environmentally-friendly sources of aluminosilicate for sequestration of aqueous and gaseous pollutants: A review. J. Cleaner Prod. 208, 1131–1147.

Kumar, A., Guo, C., Sharma, G., Pathania, D., Naushad, M., Kalia, S., Dhiman, P., 2016. Magnetically recoverable ZrO_2/Fe_3O_4/chitosan nanomaterials for enhanced sunlight driven photoreduction of carcinogenic Cr(vi) and dechlorination & mineralization of 4-chlorophenol from simulated waste water. RSC Adv. 6 (16), 13251–13263.

Kumar, S., Koh, J., 2012. Physiochemical, Optical and Biological Activity of Chitosan-Chromone Derivative for Biomedical Applications. Int. J. Mol. Sci. 13 (5).

Lei, H., Zhang, H., Zou, Y., Dong, X., Jia, Y., Wang, F., 2019. Synergetic photocatalysis/piezocatalysis of bismuth oxybromide for degradation of organic pollutants. J. Alloy. Compd. 809, 151840.

Mehrabian, M., Esteki, Z., 2017. Degradation of methylene blue by photocatalysis of copper assisted ZnS nanoparticle thin films. Optik 130, 1168–1172.

Meng, X., Khoso, S.A., Wu, J., Tian, M., Kang, J., Liu, H., Zhang, Q., Sun, W., Hu, Y., 2019. Efficient COD reduction from sulfide minerals processing wastewater using Fenton process. Miner. Eng. 132, 110–112.

Motshekga, S.C., Ray, S.S., Onyango, M.S., Momba, M.N.B., 2015. Preparation and antibacterial activity of chitosan-based nanocomposites containing bentonite-supported silver and zinc oxide nanoparticles for water disinfection. Appl. Clay Sci. 114, 330–339.

Naushad, M., 2014. Surfactant assisted nano-composite cation exchanger: development, characterization and applications for the removal of toxic Pb^{2+} from aqueous medium. Chem. Eng. J. 235, 100–108.

Naushad, M., Sharma, G., Alothman, Z.A., 2019. Photodegradation of toxic dye using Gum Arabic-crosslinked-poly(acrylamide)/Ni$(OH)_2$/FeOOH nanocomposites hydrogel. J. Cleaner Prod. 241, 118263.

Packirisamy, R.G., Govindasamy, C., Sanmugam, A., Venkatesan, S., Kim, H.-S., Vikraman, D., 2019. Synthesis of novel $Sn_{1-x}Zn_xO$-chitosan nanocomposites: structural, morphological and luminescence properties and investigation of antibacterial properties. Int. J. Biol. Macromol. 138, 546–555.

Pinto, R.J.B., Daina, S., Sadocco, P., Neto, C.P., Trindade, T., 2013. Antibacterial Activity of Nanocomposites of Copper and Cellulose. Biomed Res. Int. 2013, 6.

Priya, M., Jeyanthi, J., 2019. Removal of COD, oil and grease from automobile wash water effluent using electrocoagulation technique. Microchem. J. 150, 104070.

Prusty, K., Swain, S.K., 2018. Nano silver decorated polyacrylamide/dextran nanohydrogels hybrid composites for drug delivery applications. Mater. Sci. Eng., C 85, 130–141.

Rabel, A.M., Namasivayam, S.K.R., Prasanna, M., Bharani, R.S.A., 2019. A green chemistry to produce iron oxide – Chitosan nanocomposite (CS-IONC) for the upgraded bio-restorative and pharmacotherapeutic activities - Supra molecular nanoformulation against drug-resistant pathogens and malignant growth. Int. J. Biol. Macromol. 138, 1109–1129.

Regiel-Futyra, A., Kus-Liśkiewicz, M., Sebastian, V., Irusta, S., Arruebo, M., Kyzioł, A., Stochel, G., 2017. Development of noncytotoxic silver–chitosan nanocomposites for efficient control of biofilm forming microbes. RSC Adv. 7 (83), 52398–52413.

Rupa, A.V., Manikandan, D., Divakar, D., Sivakumar, T., 2007. Effect of deposition of Ag on TiO2 nanoparticles on the photodegradation of Reactive Yellow-17. J. Hazard. Mater. 147 (3), 906–913.

Sharma, G., Gupta, V.K., Agarwal, S., Bhogal, S., Naushad, M., Kumar, A., Stadler, F.J., 2018a. Fabrication and characterization of trimetallic nano-photocatalyst for remediation of ampicillin antibiotic. J. Mol. Liq. 260, 342–350.

Sharma, G., Kumar, A., Devi, K., Sharma, S., Naushad, M., Ghfar, A.A., Ahamad, T., Stadler, F.J., 2018b. Guar gum-crosslinked-Soya lecithin nanohydrogel sheets as effective adsorbent for the removal of thiophanate methyl fungicide. Int. J. Biol. Macromol. 114, 295–305.

Sharma, G., Kumar, A., Sharma, S., Naushad, M., Prakash Dwivedi, R., Alothman, Z.A., Mola, G.T., 2019. Novel development of nanoparticles to bimetallic nanoparticles and their composites: a review. J. King Saud Univ. – Sci. 31 (2), 257–269.

Sharma, G., Naushad, M., Al-Muhtaseb, A.a.H., Kumar, A., Khan, M.R., Kalia, S., Shweta, Bala, M., Sharma, A., 2017. Fabrication and characterization of chitosan-crosslinked-poly(alginic acid) nanohydrogel for adsorptive removal of Cr(VI) metal ion from aqueous medium. Int. J. Biol. Macromolecules 95, 484-493

Sharma, G., Naushad, M., Pathania, D., Mittal, A., El-desoky, G.E., 2015. Modification of Hibiscus cannabinus fiber by graft copolymerization: application for dye removal. Desalin. Water Treat. 54 (11), 3114–3121.

Sharma, G., Pathania, D., Naushad, M., Kothiyal, N.C., 2014. Fabrication, characterization and antimicrobial activity of polyaniline Th(IV) tungstomolybdophosphate nanocomposite material: Efficient removal of toxic metal ions from water. Chem. Eng. J. 251, 413–421.

Sharma, G., Sharma, S., Kumar, A., Al-Muhtaseb, A.a.H., Naushad, M., Ghfar, A.A., Mola, G.T., Stadler, F.J., 2018c. Guar gum and its composites as potential materials for diverse applications: a review. Carbohydrate Polymers 199, 534-545

Singh, N.P., Gupta, V.K., Singh, A.P., 2019. Graphene and carbon nanotube reinforced epoxy nanocomposites: a review. Polymer 180, 121724.

Sui, B., Li, Y., Yang, B., 2019. Nanocomposite hydrogels based on carbon dots and polymers. Chin. Chem. Lett.

Travan, A., Pelillo, C., Donati, I., Marsich, E., Benincasa, M., Scarpa, T., Semeraro, S., Turco, G., Gennaro, R., Paoletti, S., 2009. Non-cytotoxic Silver Nanoparticle-Polysaccharide Nanocomposites with Antimicrobial Activity. Biomacromolecules 10 (6), 1429–1435.

Vanaamudan, A., Sadhu, M., Pamidimukkala, P., 2018. Chitosan-Guar gum blend silver nanoparticle bionanocomposite with potential for catalytic degradation of dyes and catalytic reduction of nitrophenol. J. Mol. Liq. 271, 202–208.

Zhang, J., Wang, A., 2010. Adsorption of Pb(II) from Aqueous Solution by Chitosan-g-poly(acrylic acid)/Attapulgite/Sodium Humate Composite Hydrogels. J. Chem. Eng. Data 55 (7), 2379–2384.

Zhang, J., Zhang, L., Zhou, S., Chen, H., Zhong, H., Zhao, Y., Wang, X., 2014. Magnetically separable attapulgite-TiO_2-Fe_xO_y composites with superior activity towards photodegradation of methyl orange under visible light radiation. J. Ind. Eng. Chem. 20 (5), 3884–3889.